The Journal of Neuroscience, February 1992, 12(2): 454–466

Autoradiographic Localization of Voltage-dependent Sodium Channels on the Mouse Neuromuscular Junction Using ^{125}I-α Scorpion Toxin. II. Sodium Channel Distribution on Postsynaptic Membranes

Jean-Louis Boudier,[1] Therese Le Treut,[1] and Emmanuel Jover[2]

[1]Laboratoire de Biologie Cellulaire-Histologie and [2]Laboratoire de Biochimie, U.A. CNRS 1179, Faculté de Médecine Nord de Marseille, 13326 Marseille Cedex 15, France

A radioiodinated α-scorpion toxin (toxin II from *Androctonus australis* Hector) (αScTx) was used as a probe for EM autoradiography to study the distribution of voltage-dependent sodium channels (Na^+ channel) on the postsynaptic side of the mouse neuromuscular junction. Silver grain distribution was analyzed by the cross-fire method to assess the relative Na^+ channel density in each membrane domain measured by stereology. This analysis showed that the maximum Na^+ channel density was located on the edge of the synaptic gutter, where it reached about twice the mean density in the postsynaptic fold membrane. Na^+ channel densities have been calculated using ACh receptor (AChR) density in fold crests as reference. Sodium channel density on the edge of the synaptic gutter was estimated at about 5000/μm^2. Sodium channel distribution in the postsynaptic folds was compard to AChR distribution using density distribution analysis (Fertuck and Salpeter, 1976). The results confirmed that, as already observed by immunogold labeling (Flucher and Daniels, 1989), there are no Na^+ channels on fold crests. Na^+ channels are located in the rest of the fold membrane (bottom) and may be distributed according to two possible models. In the first, density would be uniformly high, although lower than on the gutter edge. In the second, density would decrease from the crest border, where the value was that of the gutter edge, to the fold end, where the value would be 50% lower. Based on the latter model, which was the "best-fit model," we propose that the postsynaptic membrane includes two domains. The first is the fold crest, which contains almost exclusively AChRs. This domain is devoted to reception–transduction of the chemical signal. The second includes both the fold bottom membrane and the perisynaptic membrane. Sodium channel density is highest along the crest border and decreases moving away. Its functions are the integration of postsynaptic potentials and generation–conduction of the muscle action potential.

The postsynaptic membrane of the vertebrate neuromuscular junction (NMJ) is the site of the transduction of a chemical signal (ACh release) into an action potential able to propagate over the muscle surface and trigger contraction (reviewed by McArdle, 1984). Although the first step of this transduction involves activation of ACh receptors (AChRs), which produce a synaptic potential, the generation and propagation of the muscle action potential depend on voltage-sensitive Na^+ channels. The postsynaptic membrane is a highly organized structure at both microscopic and molecular levels. In synaptic gutters, the membrane is considerably infolded. The fold crest membrane appears "thickened" (Birks et al., 1960; Cartaud et al., 1981; Sealock, 1982). The density of AChRs in these crest areas is very high (about 10,000/μm^2) (Heuser and Salpeter, 1979; Salpeter et al., 1984). Sodium channels are also distributed at higher densities in the synaptic and perisynaptic zones than on the muscle extrasynaptic surface, as shown by electrophysiological studies (Almers et al., 1983; Betz et al., 1984; Beam et al., 1985; Caldwell et al., 1986; Caldwell and Milton, 1988) and microscopic studies (Angelides, 1986; Dreyfus et al., 1986; Ariyasu et al., 1987; Haimovich et al., 1987; Boudier et al., 1988; Flucher and Daniels, 1989; Le Treut et al., 1990). Caldwell et al. (1986) claimed that Na^+ channel density was several thousand per square micrometer at the end-plate. From there, Na^+ channel density decreases smoothly and reaches extrasynaptic density at a distance of 50 μm (Le Treut et al., 1990) or 200 μm (Beam et al., 1985; Caldwell et al., 1986). Immunogold EM labeling revealed Na^+ channels in the fold bottom and the perisynaptic membrane but not in the fold crests where the AChRs are located (Flucher and Daniels, 1989). Thus, like AChRs, Na^+ channel distribution on the end-plate appears highly organized. It is an important parameter in the generation and initial propagation of the muscle action potential. The aim of the present article is to obtain new insights into Na^+ channel distribution on the postsynaptic membrane.

Neurotoxins have proven to be valuable tools for the Na^+ channel study. Among them, radioiodinated scorpion toxins have been used for autoradiographic localization of Na^+ channels on nerve cells (Boudier et al., 1985; Cau et al., 1985) and muscle tissue (Boudier et al., 1988; Le Treut et al., 1990). At least five different neurotoxin-binding sites have been described on the Na^+ channel (Catterall, 1980; Couraud et al., 1982; Poli

Received Oct. 31, 1990; revised Aug. 29, 1991; accepted Sept. 13, 1991.

This investigation was performed with the technical assistance of Jeannine Bottini and Anne-Marie Athouel and was supported by INSERM (U.172) and by grants from the Association Française contre les Myopathies. We thank Dr. M.-F. Martin-Eauclaire for giving us the scorpion toxin, Dr. N. Martin-Moutot for the radioiodination of some toxin batches, Dr. P. Cau for allowing us to use some of his cross-fire programs and for helpful advice in stereology, and Drs. P. Bougis and P. Marchot for donating radioiodinated snake toxin. We are also grateful to D. Angaut-Petit, F. Couraud, B. Dargent, P. David, A. Mallart, and M. Seagar for their useful comments and criticisms.

Correspondence should be addressed to Dr. Jean-Louis Boudier, Laboratoire Biologie Cellulaire-Histologie, Faculté de Médecine Nord, Boulevard Pierre-Dramard, 13326 Marseille Cedex 15, France.

et al., 1986). α-Scorpion toxins (αScTx) bind to site 3, located between segments S5 and S6 of domains I and IV of the α-subunit, which shares the ion channel (Thomsen and Catterall, 1989). Binding of the αScTx slows down the channel inactivation and is highly potential dependent (Catterall, 1980).

In a previous report (Boudier et al., 1988), we reported the localization of Na^+ channels on the mouse NMJ using ^{125}I-αScTx as a probe. Since that study dealt primarily with the Na^+ channel distribution on presynaptic structures, the EM autoradiography (EM-ARG) was performed on preparations submitted to a prolonged postincubation rinse to wash out toxin from muscle binding sites. The postsynaptic membrane was not labeled, and Na^+ channels were detected on junctional glial cells. In the present study, however, EM-ARG was performed on briefly rinsed muscles in order to study the Na^+ channel distribution on the postsynaptic membrane. Labeling distribution was first analyzed by the cross-fire method (Blackett and Parry, 1973). Then, the distribution of ^{125}I-αScTx–binding sites on the postsynaptic folds was compared to the distribution of AChRs visualized with a radioiodinated α-neurotoxin (^{125}I-αNTx), using density distribution analysis (Salpeter et al., 1969).

Materials and Methods

Toxins. Toxin II from the venom of *Androctonus australis* Hector (αScTx) was obtained from M.-F. Martin (Laboratoire de Biochimie, Faculté de Médecine-Secteur Nord, Marseille, France). α-ScTx was radioiodinated as previously described (Martin et al., 1987); activity obtained was 1300–1500 Ci/mmol. Binding of this scorpion toxin has already been extensively characterized (Couraud et al., 1978; Jover et al., 1978). Radioiodinated toxin from the snake *Naja mossambica mossambica* (αNTx) (1800–2000 Ci/mmol; 95% monoiodinated) was a gift from P. Marchot (same address). This short snake α-neurotoxin has almost the same M_r as αScTx (Rochat et al., 1974). It binds on the same two independent sites of the AChR as α-bungarotoxin (K_{d1} = 7 pM; K_{d2} = 51 pM). Affinity of native and monoiodinated αNTx is not significantly different (Marchot et al., 1988).

Muscle–nerve preparation. The mouse hemithorax was excised and placed in a Petri dish, under a continuous flow of a solution containing 137 mM NaCl, 5 mM KCl, 2 mM $CaCl_2$, 0.8 mM $MgCl_2$, 11 mM glucose, 25 mM HEPES, and TRIS base to obtain pH 7.2, saturated with 95% O_2, 5% CO_2. The Triangularis sterni muscle was then exposed as previously described (McArdle et al., 1981).

Toxin incubation. Preparations were incubated at room temperature (18–20°C) for 30 min in an Na^+- and Ca^{2+}-free medium containing 140 mM choline chloride, 5.4 mM KCl, 0.8 mM $MgCl_2$, 10 mM glucose, 25 mM HEPES, and TRIS base to obtain pH 7.2. Each experiment included at least two preparations: one was incubated with 1 nM of ^{125}I-αScTx ("total binding" sample), and the other aimed at labeling of nonspecific sites incubated with 1 nM ^{125}I-αScTx plus 0.2 μM of native toxin ("nonspecific binding" sample). Radioiodinated αNTx was incubated at 0.5 nM for total binding and at 0.5 nM plus 0.1 μM native toxin for nonspecific binding. Incubation was followed by three brief rinses of about 20 sec each (5 × 30 sec for αNTx) using ice-cooled incubation medium without any toxin. Then the preparations were transferred into the fixation solution (2.5% glutaraldehyde in the incubation medium) for 1 hr at room temperature.

Tissue processing and preparation of autoradiograms. After several brief rinses in PBS, muscles were cut into blocks, postfixed in 2% OsO_4 solution, dehydrated in ethanol, and embedded in Epon. Ultrathin sections were collected onto collodion-coated slides. ARG was performed by the dipping method (Larra and Droz, 1970). The emulsion Ilford L4 was developed in Kodak Microdol X after 27–65 d of exposure at 4°C.

Quantitative analysis. At EM level, radiation scatter prevents precise localization of the radioactive molecule (source) according to individual grain position. The cross-fire analysis (Blackett and Parry, 1973, 1977; Downs and Williams, 1978; Salpeter et al., 1978; Williams and Downs, 1978) allows assessment of the source density for each substructure by adjustment of the result of a simulation ("cross-fire" matrix of hypothetical, generated source–grain sets systematically distributed over the tissue) to the distribution of real observed grains (observed grain vector).

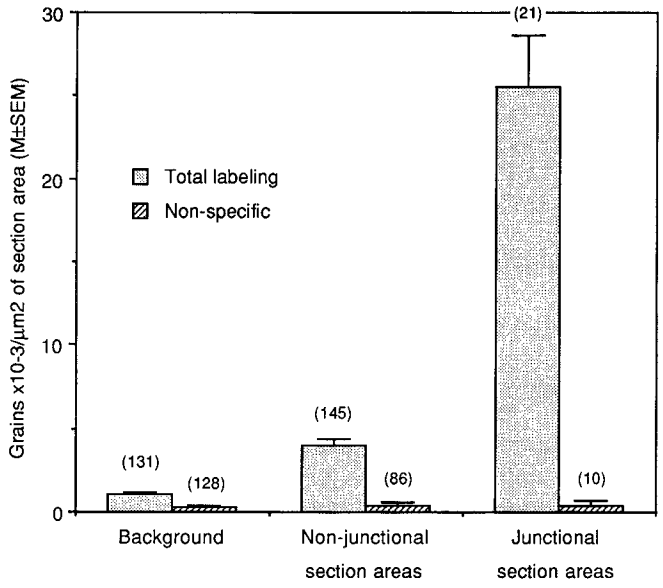

Figure 1. EM-ARG. Silver grain counts on muscles incubated either with 1 nM ^{125}I-αScTx (*Total labeling*) or with 1 nM ^{125}I-αScTx plus 0.2 μM of unlabeled αScTx (*Non-specific*). Grains were counted in section areas sampled systematically. Counts were designated as "junctional" for areas containing an NMJ profile, "non-junctional" if they did not, and "background" if the section area was tissue free. The number of areas is indicated in *parentheses*. Note the low level of nonspecific labeling and the predominant labeling of NMJs.

This analysis was performed in order to obtain the general source distribution over the NMJs in αScTx-incubated preparations. The density distribution method ("histogram" method) (Salpeter et al., 1969; Fertuck and Salpeter, 1976) was used on both αScTx- and αNTx-labeled preparations in order to study the source distribution over the postsynaptic fold membrane. Both methods were performed on micrographs viewed at a magnification of 26,140× checked with a calibration grating replica.

First, the background and the global labeling of muscle were measured by grain counting at 7900× magnification using the quadrat method (Williams, 1977). The background was counted on section areas free of tissue. It was consistently low. Mean grain number per square micrometer of section area was $4.72 \times 10^{-4} \pm 2.01 \times 10^{-4}$ (±SEM); the maximum was 10.5×10^{-4} (Fig. 1). Section areas containing tissue were divided into "junctional" if they contained an NMJ profile and "nonjunctional" if not. In total labeling experiments, signal-to-background ratios ranged from 4 to 6 for nonjunctional areas and 24 to 50 for junctional areas (Fig. 1).

Cross-fire analysis. This method was used here almost exactly as described in a previous study of Na^+ channels on NMJs (Boudier et al., 1988). Particularly, 47-nm-radius circles (1.25 mm on micrographs) were again used to attribute grains and sources to compartments instead of the center of the grain, as classically described. The circle radius was chosen by trial and error to allow both a significant sampling of the membranes and, in practice, separate sampling of the presynaptic membrane and the top of the postsynaptic folds. However, in membrane compartments, grains were attributed to a membrane-associated volume rather than to the membrane surface area itself. Thus, to express source densities per membrane surface area unit, an adjustment calculated from stereological data was introduced (see below). In the present study, the half-distance (HD) was assessed at 120 nm (HD was defined by Salpeter et al., 1969, as the distance from a radioactive line source that contains 50% of the grains derived from the source). This HD was set from a hot-line experiment (Salpeter et al., 1977). Overlays with generated source–grain sets were drawn consequently. Adjustment of the cross-fire matrices was computed using an iterative method (Cau, 1988).

Stereology and source density calculation. These calculations were performed on the same micrographs used for cross-fire analysis and at the same magnification. The reference area was estimated by point

counting, and the membrane perimeters, by counting intercepts with lines of a square test grid (15 points; test line length, 158.5 cm or 519.5 cm for analysis of either αScTx- or αNTx-incubated muscles, respectively). Means and errors were calculated using the standard stereological formulas (Weibel, 1979). Then, the volume of reference and membrane surface areas were obtained by multiplying the cross-section area and the membrane perimeters, respectively, by section thickness estimated using the fold method (Small, 1968) (77.1 ± 11.9 nm, mean ± SD).

The optimized source densities (OSDs) obtained by adjustment of the cross-fire matrix are expressed in units of generated source (Salpeter et al., 1978). In order to obtain OSD per membrane surface area unit, the generated source density (GSD) per square micrometer of membrane surface area (see Table 4) is first calculated by dividing the total generated source number (see Table 2) by the respective membrane surface area in each membrane compartment (see Table 4). Then, OSDs were multiplied by GSD/μm^2 in order to obtain the OSD/μm^2 of membrane surface area (see Table 4).

Quantitation of scorpion toxin–binding sites. The derivation of the binding site density from the source density was performed using the following formula obtained from Fertuck and Salpeter (1974, 1976) and Land et al. (1977):

$$\text{Binding site density}/\mu m^2 = \frac{G \times d \times A}{124{,}800 \times S_0 \times C \times T},$$

where G = OSD/μm^2; d = photographic sensitivity (=100/efficiency in percent); A = Avogadro's number (6.023×10^{20} molecules/mmol); S_0 = specific activity at the time of toxin labeling; $C = 2.22 \times 10^{12}$ disintegrations/min; and $T = [1 - (e^{-0.01155t_e}) \times (e^{-0.01155t_0})]$, where t_e is the exposure time and t_0 is the time between the labeling of the toxin and the beginning of exposure (in days). This binding site density was then corrected by the site occupation rate to obtain the absolute toxin binding site density.

This formula was first used to calculate the photographic sensitivity in the AChR labeling experiment using ^{125}I-αNTx. The source density on the fold crests was calculated at 7.29 ± 1.73 sources/μm^2 (mean ± SD) by attributing all the grains within 10 HD from fold crests to them, their membrane surface area being evaluated by stereology (see above). The αNTx binding site density was assumed to be equal to the α-bungarotoxin site density published by Salpeter et al. (1984; i.e., 17,000/μm^2). In these conditions, the sensitivity was 909.1, which corresponds to an efficiency of 0.11%. This sensitivity value has been used in the formula to calculate the αScTx binding site density/μm^2 from OSD/μm^2.

Density distribution method. This analysis was performed as described by Salpeter et al. (1969) and Fertuck and Salpeter (1976). A putative line source was traced, joining the tops of the folds (and thus parallel to the presynaptic nerve ending membrane). Each silver grain located at less than 10 HD distance (1.2 μm; 32 mm on micrograph) from this line or from any part of the folds was considered. The shortest distance between the center of the grain to the line was recorded. Then, random points were generated in the area of consideration with a square grid, and point-to-line distances were recorded. Finally, the apparent fold length was also recorded. Data associated with apparent fold length shorter than 0.4 μm or longer than 1 μm were discarded as presumably obtained from sections not perpendicular to the fold axis. All other distances were normalized for a fold length of 0.72 μm (6 HD). Separate histograms were constructed for grain-line and point-line distances with bins of 1 HD in width. The grain density histogram was obtained by dividing each bin in the grain number histogram by the same bin in the point number histogram. Then, assumptions were made on the source distribution on folds and related theoretical models of grain distribution were built using the line-source or the band-source distributions published by Salpeter et al. (1969, 1977). Finally, the theoretical grain distributions were tested against the observed one with a χ^2 test.

Results

Labeling of NMJs

Global quantitative analysis of muscle labeling is presented in Figure 1. In total binding preparations, "junctional" section areas were about 6.5× more labeled than "nonjunctional" ones. In nonspecific binding preparations, no significant difference was seen between junctional and nonjunctional areas. Maximum nonspecific labeling was about 10% of the total.

These results were illustrated by observation of αScTx total binding preparations (Fig. 2). Few silver grains were observed on muscle fiber surfaces. Conversely, almost all the NMJ profiles were labeled by grains whose number should vary from one to two dozen. A few NMJ profiles were not labeled at all. Nonspecific binding preparations never showed such labeling of NMJs, and grains were rare on other areas. These findings are in agreement with our previous claim that αScTx-binding Na^+ channels are mainly localized on NMJs (Boudier et al., 1988).

Observation of NMJs at higher magnification in total binding preparations showed that the grains were scattered over the NMJs (Fig. 3*A*), and they were obviously more numerous on the postsynaptic side. Although sources cannot be assessed to individual grain positions, labeling with αScTx (Fig. 3*A*) exhibited a clearly different pattern from the one obtained with αNTx (Fig. 3*B*). With the latter toxin, more grains were grouped on postsynaptic fold crests.

αScTx binding and Na^+ channel distribution on the NMJs

Cross-fire analysis was performed on preparations incubated in 1 nM of ^{125}I-αScTx (total binding). Tissue was divided into 10 putative grain and source compartments as already described (Boudier et al., 1988). Table 1 shows the different compartments. Primary cross-fire data are displayed in Table 2. As the sources were systematically distributed, the generated source density is equivalent to the volume density of each compartment in the micrographs used. Sampling with a small circle also allowed assessment of volume density of membrane compartments. Observed and generated grain distributions are significantly different, as shown by the χ^2 test. Thus, observed grains were not randomly distributed on the NMJs.

This primary model with 10 source and grain compartments was tested. The OSDs, expressed in units of generated source (Salpeter et al., 1978), and related errors were calculated by adjustment of generated to observed grains. The accuracy of OSDs was evaluated using a χ^2 test to compare the grain distribution calculated from OSDs with observed grain distribution. The χ^2 value was 5.62. OSD in muscle, axon, axon membrane, and intercellular space was close to zero. Following the "iterative deconvolution procedure" (Downs and Williams, 1978; Williams and Downs, 1978), the primary model was then modified by suppression of empty source compartments. These new models were systematically tested. The final best-fit model has 8 source and 10 grain compartments, axon interior and intercellular space being suppressed as source compartments (Table 3). The χ^2 test is slightly improved. All the membrane compartments except the presynaptic axon membrane were significantly labeled, in contrast with nonmembrane compartments (muscle and glia interiors).

As mentioned above, the source densities of membrane compartments are related to membrane-associated volumes. The membrane surface area inside each membrane compartment of the cross-fire analysis was estimated by stereology (Table 4), allowing the number of generated sources per membrane surface area and finally the OSD per membrane surface area to be calculated. Two important differences between source density per membrane surface area and binding site density, that is, from αScTx-binding Na^+ channel density, should be stressed. First, each membrane type was assumed to be uniformly labeled, which is not true at least on postsynaptic membrane folds (see below) and perisynaptic membrane (Le Treut et al., 1990). Consequently, values obtained in these compartments were mean

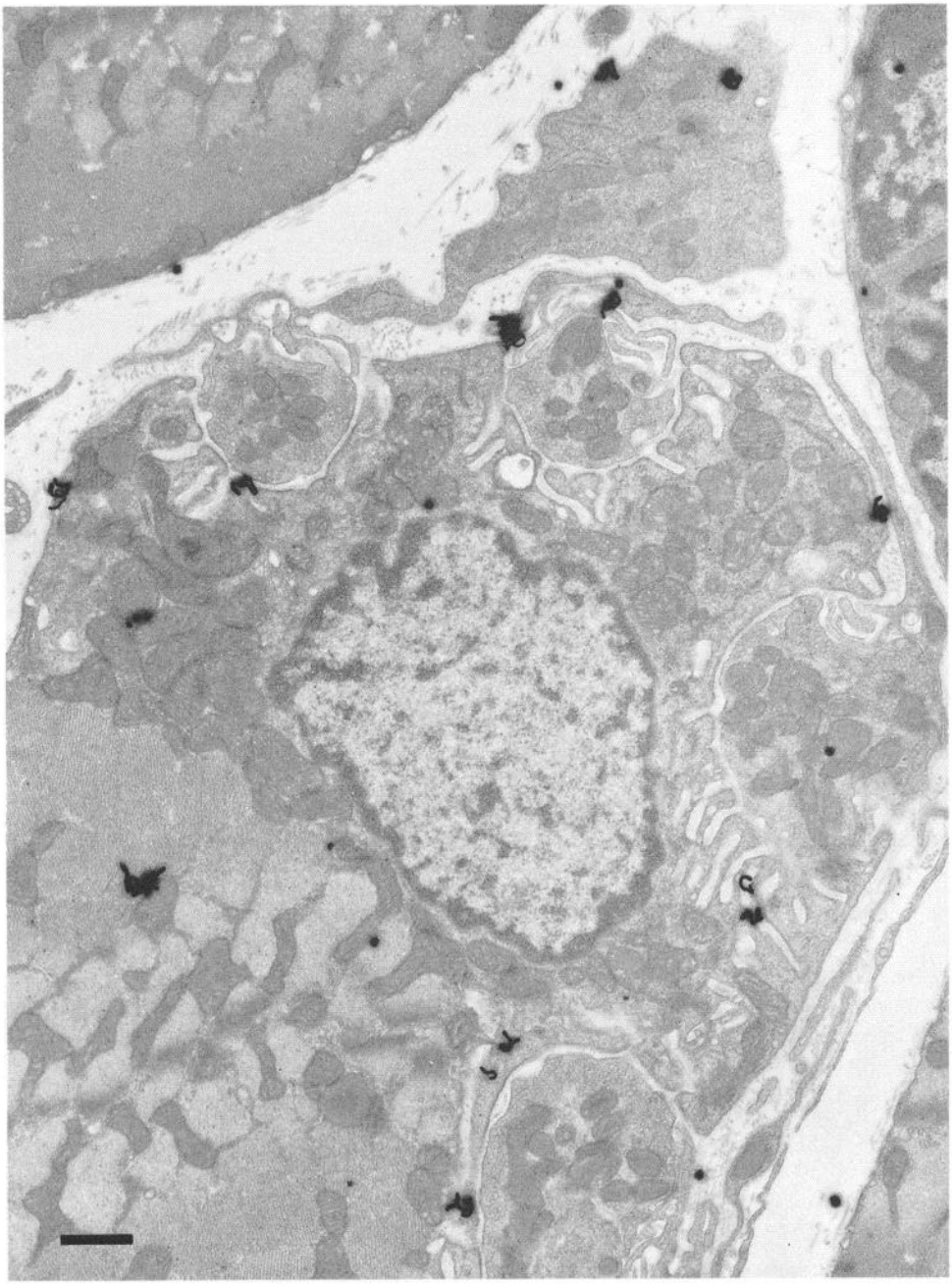

Figure 2. EM-ARG localization of αScTx-labeled voltage-sensitive sodium channels: transverse section of muscle showing the usual labeling level of NMJ profiles. Incubation was with 1 nM ^{125}I-αScTx (total binding). Magnification, 11,500×. Scale bar, 1 μm.

densities. Second, OSD is proportional but not equal to the binding site density. Fertuck and Salpeter expressed this relationship in a formula published in 1974 (see Materials and Methods).

Despite these limits, however, OSD per membrane surface area could be compared. Mean Na^+ channel density on the perisynaptic muscle membrane appeared to be about twofold higher than on the postsynaptic folds (Table 4). Source density on the glial membrane appeared largely significant. The glial and axonal membranes, in areas where they could not be analyzed separately, displayed a higher source density than glial membrane alone. However, density in the presynaptic nerve membrane facing the folds was low (not nil, as suppression of this compartment increased the χ^2).

Na^+ channel density

In theory, the relationship between absolute Na^+ channel density and the source density given in Table 4 depends on site occupation rate, specific activity of the toxin, exposure time, and efficiency of the detection system. A formula published by Fertuck and Salpeter (1974, 1976; also appearing in Land et al., 1977, in a different form) allows conversion of grain density into radioactive site density according to these parameters (see Materials and Methods). The K_d of αScTx for adult muscle Na^+ channel has been estimated at ≈1 nM from binding (Sherman et al., 1983) and electrophysiological (Duval et al., 1989) studies. Since incubation was performed with 1 nM ^{125}I-αScTx, the mean site occupation rate was set at 0.5. The efficiency of the detection

Table 1. Tissue division into grain and source compartments for the cross-fire analysis

Tissue division	Definition
1. Muscle int.	Internal space delimited by the muscle cell–surface membrane including nucleus and cytoplasmic organelles
2. Muscle mmb.	Muscle cell–surface membrane except the postsynaptic zone (folds)
3. Fold mmb.	Muscle postsynaptic membrane (whole folds including crests)
4. Glia int.	Internal space delimited by the surface membrane of identified glial cells including cytoplasmic organelles
5. Glia mmb.	Surface membrane of glial cells identified by close contact with axon and/or presence of a basal lamina
6. Glia + Ax. mmbs.	Parts of glial and axonal membranes facing together and being in close contact
7. Axon int.	Internal space delimited by the axon terminal membrane including cytoplasmic organelles
8. Axon mmb.	Presynaptic part of the axon terminal membrane, facing the muscle postsynaptic membrane
9. Unident. process.	Membrane and interior of thin cell processes not formally identified
10. Intercell. space	All the external space including connective tissue with collagen and sometimes capillary blood vessel

system is very difficult to assess accurately. In the present study, this problem was overcome using AChR density as a reference value. A value of 8000–10,000 AChRs/μm^2 on the crests of postsynaptic folds is generally accepted (Salpeter, 1987). With this value, $\approx$17,000 α-bungarotoxin–binding sites/μm^2 were detected by EM-ARG (Salpeter et al., 1984). ARG efficiency was thus calculated from the αNTx labeling experiment with this α-bungarotoxin binding site density. It only was 0.11%, which is very low in comparison with other values found in the literature (Fertuck and Salpeter, 1974; Salpeter et al., 1984). Nevertheless, this efficiency has been obtained under the same conditions and on the same material as for the Na^+ channel localization. Na^+ channel densities calculated with this experimental efficiency value were high (Table 4). It should be kept in mind that the validity of these Na^+ channel densities is based on AChR density. Due to errors from the numerous calculations carried out, these values were subjected to a relatively large final error, probably higher than 30%. The perisynaptic muscle membrane bore the highest density: $\approx$5500 Na^+ channels/μm^2 ($\approx$5000 after deduction of 10% nonspecific binding), about twice the mean density on postsynaptic folds. In contrast with the high levels observed on glial and glial plus axonal membrane compartments, the Na^+ channel density on presynaptic membrane is not significant.

Distribution of αScTx-binding Na^+ channels on postsynaptic folds

This was studied by the density distribution method (Salpeter et al., 1969). The grain distribution was established relative to a reference line joining the top of the postsynaptic folds (TF-line) (Fig. 4). In the NMJs studied here, the apparent mean length of the folds was 0.73 ± 0.09 μm (mean ± SD) and the "thickened" membrane, which contains almost all of the AChRs (reviewed by Salpeter, 1987), extended 0.19 ± 0.05 μm (mean ± SD) down the folds. For the following study, the fold length was set at 6 HD (0.72 μm), and the limit of the thickened membrane, at 2 HD (0.24 μm). The thickened top part of the folds is referred to as the "crest," and the nonthickened part, beginning 0.24 μm from the TF-line and extending to the lower end, as the "bottom" (Fig. 4).

The procedure was tested on preparations incubated with 0.5

Table 2. Original "cross-fire" table

Grain compartments	1. Muscle int.	2. Muscle mmb.	3. Fold mmb.	4. Glia int.	5. Glia mmb.
Source compartments					
1. Muscle int.	5595	55	126	1	5
2. Muscle mmb.	43	34	2	0	3
3. Fold mmb.	158	6	539	2	10
4. Glia int.	1	1	2	423	68
5. Glia mmb.	7	7	5	66	266
6. Glia + Ax. mmbs.	1	0	1	8	18
7. Axon int.	15	1	32	6	21
8. Axon mmb.	6	0	38	1	5
9. Unident. process.	1	0	0	0	8
10. Intercell. space	61	55	21	35	103
Total generated grains	5888	159	766	542	507
Observed grains	163	43	230	46	78
Normalized generated	336.9	9.10	43.82	31.01	29.01
χ^2	89.73	126.4	790.9	7.25	82.75

See Table 1 for abbreviations.

* df = 9; $p < 0.001$.

Table 3. Adjustment of the final model to the observed grain distribution: calculated source density and test of the adjustment accuracy

Compartments	OSD Mean	OSD ±SD	Grain number Calculated	Observed	Calculated normalized	χ^2 test
1. Muscle int.	0.01	0.002	165.66	163	164.76	0.02
2. Muscle mmb.	1.04	0.22	39.91	43	39.69	0.28
3. Fold mmb.	0.41	0.04	225.19	230	223.97	0.16
4. Glia int.	0.06	0.02	44.38	46	44.14	0.08
5. Glia mmb.	0.21	0.05	76.68	78	76.27	0.04
6. Glia + Ax. mmbs.	0.55	0.24	20.97	24	20.85	0.48
7. Axon int.	Suppressed		33.03	23	32.85	2.96
8. Axon mmb.	0	0.19	14.05	14	13.97	0
9. Unident. process.	0.10	0.04	10.19	11	10.13	0.07
10. Intercell. space	Suppressed		89.86	84	89.37	0.32
Total			719.90	716	716	4.40*

See Table 1 for abbreviations.
* df = 9; $p > 0.75$.

nM of ^{125}I-αNTx, which binds the AChRs. The observed grain distribution has been compared with a line source distribution (Salpeter et al., 1977) centered on the TF-line (Fig. 5), that is, AChRs located exclusively on the top of crests. As expected, these two distributions did not fit. The observed distribution was almost identical to the classical one published by Fertuck and Salpeter (1976). Most of the labeling was concentrated on the top of crests, but an additional component was noted in the muscle direction, due to an AChR-rich zone extending about 200 nm down the folds (Fertuck and Salpeter, 1976; Salpeter et al., 1984).

The grain distribution obtained with ^{125}I-αScTx–binding Na^+ channels appeared to be complementary to that obtained with ^{125}I-αNTx bound to AChRs. Labeling was greatest toward the bottom (Fig. 5). Source distributions were elaborated from several hypothetical Na^+ channel localizations and compared with the observed one using the χ^2 test (Table 5). The related models of source distribution have been built using band sources (Salpeter et al., 1969, 1977) of equal source density and different widths. They have been used either singly or superimposed in order to simulate uneven densities (Fig. 4). The possibility of uniform distribution of Na^+ channels over the entire fold was clearly rejected. A uniform distribution exclusively on the bottom, however, cannot be rejected. The same model with an increased density of sources in the lower half of the fold bottom did not fit. The "best-fit" model was a 4-HD-wide band source covering the bottom, with a twofold density in the upper half. The grain distribution derived from this model is presented in Figure 6*A*, and the fitting with the observed grain distribution is shown in Figure 6*B*. Models with a continuous gradient of Na^+ channel density or with density ratios up to 4 cannot be ruled out (Table 5). In the NMJ sample used here, the crest

Table 2. Continued

6. Gl. + Ax. mmbs.	7. Axon int.	8. Axon mmb.	9. Unident. process.	10. Intercell. space		Total generated sources	Source compartment volume density
0	6	7	1	54		5850	0.467
0	2	0	0	47		131	0.010
3	36	31	0	8		793	0.063
2	7	0	3	48		555	0.044
20	12	1	2	124		510	0.041
28	24	2	0	2		84	0.007
26	575	27	0	6		709	0.057
8	40	25	0	1		124	0.010
0	0	0	99	79		187	0.015
3	8	3	81	3202		3572	0.285
90	710	96	186	3571	Total	12,515	1
24	23	14	11	84	716		
5.15	40.62	5.49	10.64	204.3	716		
69.01	7.64	13.18	0.01	70.84	1257.71*		

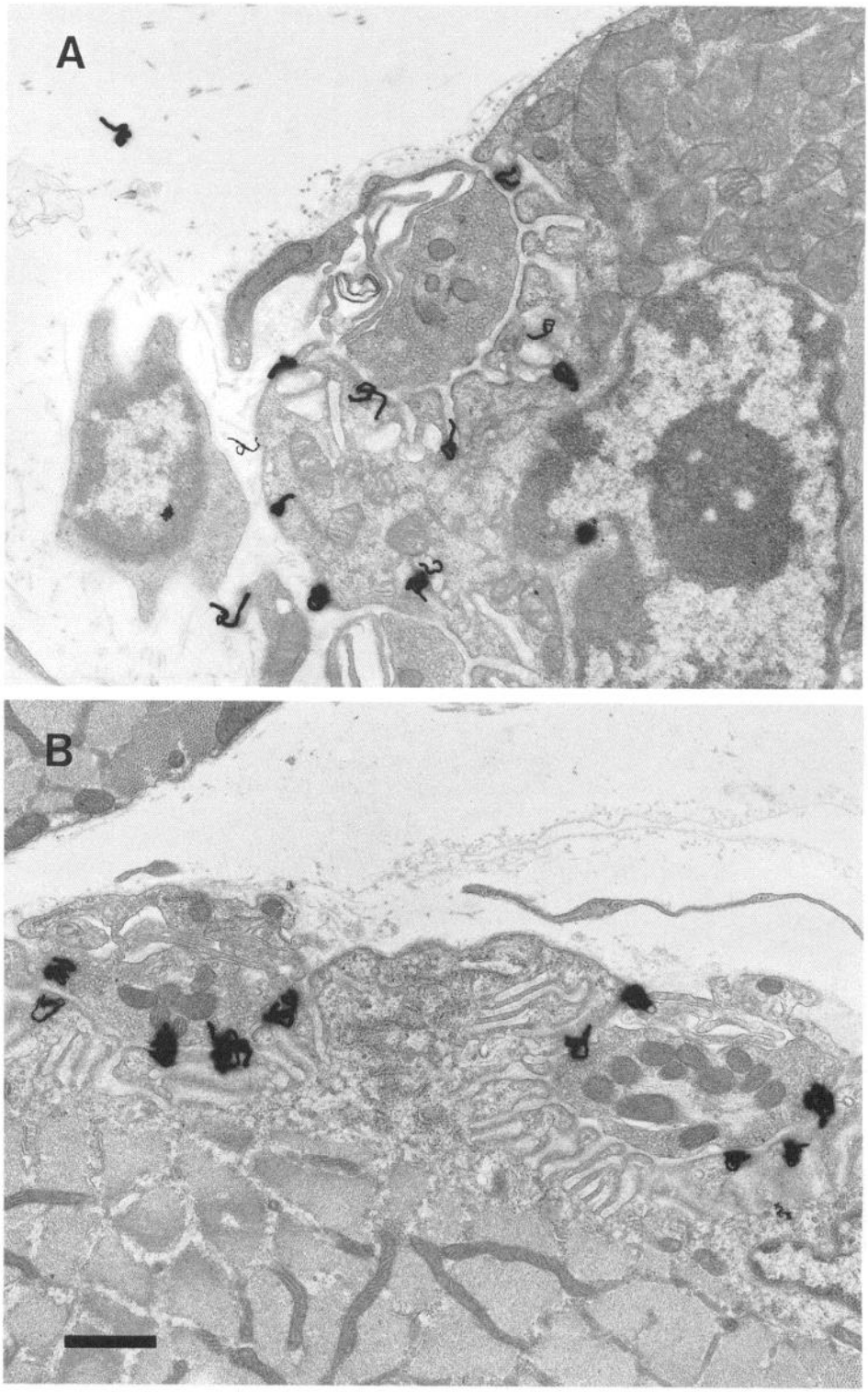

Figure 3. EM-ARG. *A,* Localization of αScTx-labeled voltage-sensitive sodium channels. Incubation was with 1 nM ^{125}I-αScTx (total binding). Silver grains were widely scattered on NMJ structures. Most were found on postsynaptic folds and perisynaptic membrane. *B,* Localization of αNTx-labeled AChRs. Incubation was with 0.5 nM ^{125}I-αNTx (total binding). Note that almost all the grains are lying on fold crests, as classically described. Magnification, 14,500×. Scale bar, 1 μm.

accounted for 30% of the total fold surface. Considering the mean Na^+ channel density on the fold to be ≈2800/μm² (after deduction of nonspecific binding), Na^+ channel density was then ≈3700/μm² on the whole fold bottom in the case of a uniform distribution (model 2 in Fig. 4 and Table 5). In the best-fit model (model 4 in Fig. 4 and Table 5), however, Na^+ channel density was ≈5000/μm² in the upper half of the bottom and ≈2500/μm² in the lower half. Thus, Na^+ channel density along the border of fold crests is identical to the density on the gutter edge in this model.

Our data indicate that αScTx-binding sodium channels are unevenly distributed on the postsynaptic membrane. Few if any are located on crests, which contain almost all the AChRs. However, Na^+ channels are most numerous on the nonthickened membrane of the fold bottom. Either they are uniformly distributed, or, according to the best-fit model, the Na^+ channel

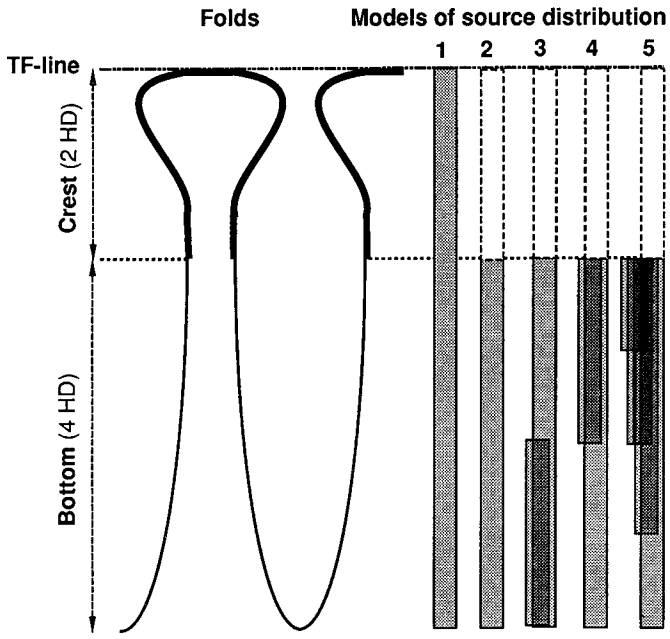

Figure 4. Theoretical model of folds used here to test several assumptions on source (^{125}I-αScTx bound to Na$^+$ channel) distributions. The TF-line is a hypothetical line joining the folds tops. The limit between the crest and the bottom has been rounded up to the next HD unit (HD = 0.12 μm). Source distribution models were built with band sources of equal density and different widths. Band sources were superimposed in some models in order to obtain compound distributions. In these models, gray levels scale roughly with the resulting source densities. Model numbers are the same as in Table 5.

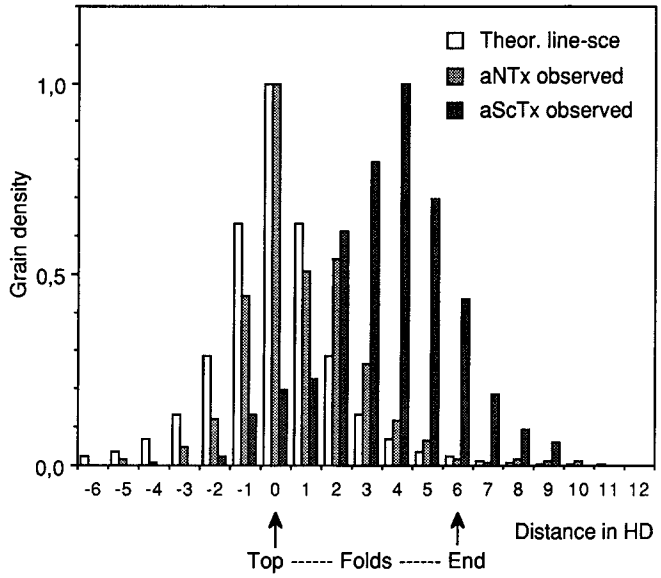

Figure 5. Grain density distribution on postsynaptic folds: comparison of hypothetical grain distribution arising from a line source located on the top of the folds (*Theor. line-sce*) and distributions observed in NMJs incubated with 0.5 nM ^{125}I-αNTx to label AChRs (*aNTx observed*) and in NMJs incubated with 1 nM ^{125}I-αScTx to label Na$^+$ channels (*aScTx observed*). The origin of the distance axis is located at the fold top. Positive values indicate a direction toward the muscle interior, and negative values, toward the nerve ending (HD = 0.12 μm). Distributions are normalized to the density unit at their peak, which coincides with the origin for aNTx and the line source. Note that the distribution of the AChR probe is concentrated on the fold crests, with a shoulder at 2 HD. The distribution of the Na$^+$ channel probe is clearly lower toward the fold ends.

density was about twofold higher in the upper than in the lower half of the fold bottom, thus reaching the same value as observed on the gutter edge.

Discussion

The distribution of Na$^+$ channels has been studied on both the pre- and postsynaptic sides of the NMJ by ARG of αScTx-binding sites. In a previous study devoted to the presynaptic side (Boudier et al., 1988), EM localization was performed on preparations after a washout of the ^{125}I-αScTx bound on the muscle membrane. Membrane domains of the postsynaptic side were not labeled. In the experiments reported here, the postincubation rinses lasted the time necessary to wash out unbound toxin, and labeling of muscle Na$^+$ channels was obtained. Mean Na$^+$ channel density appeared to be higher on the perisynaptic muscle membrane than on the postsynaptic folds. Density distribution analysis of labeling on folds showed that Na$^+$ channel and AChR distributions were different. No Na$^+$ channels were present on crests, where AChR density is very high. Further-

Table 4. Source densities per membrane surface area and conversion into Na$^+$ channel density

Mmb. compartments	Mmb. area (μm^2) Mean	±SD	Generated source/μm^2 mmb. area Mean	±SD	Optimized source/μm^2 mmb. area Mean	±SD	Na$^+$ channel/μm^2 mmb. area (total αSc Tx–binding sites/μm^2 mmb area)
2. Muscle mmb.	105.18	20.66	1.25	0.24	1.30	0.53	5580
3. Fold mmb.	447.08	78.1	1.77	0.31	0.73	0.20	3119
5. Glia mmb.	392.94	69.18	1.30	0.23	0.27	0.11	1144
6. Glia + Ax. mmbs.	61.18	12.82	1.37	0.29	0.76	0.49	3271
8. Axon mmb.	74.18	15.17	1.67	0.34	0.01	0.31	43
9. Unident. process.	105.3	20.68	1.78	0.08	0.17	0.10	741

See Table 1 for abbreviations.

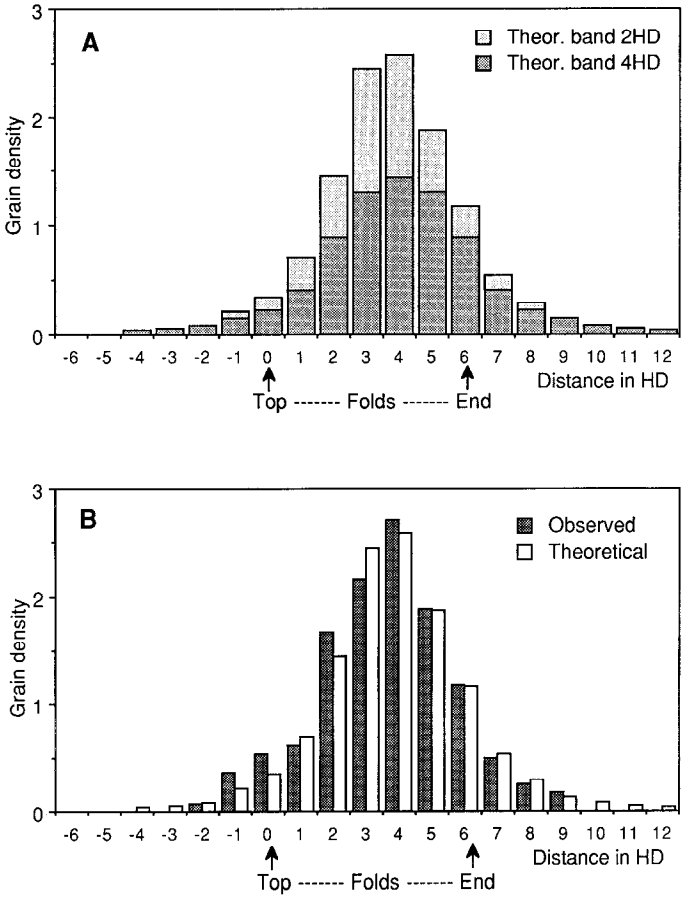

Figure 6. Grain distributions on postsynaptic folds. The origin of the distance axis is located on the fold top, and positive distances indicate a direction toward the fold ends. *A,* The "best-fit" hypothetical grain distribution arising from a compound source composed with a band 4 HD wide, located at 2–6 HD, and another superimposed band of equal source density, 2 HD wide and located at 2–4 HD. *B,* Comparison of the previous hypothetical distribution (*Theoretical*) with the observed grain distribution. Distributions are normalized to the observed total density.

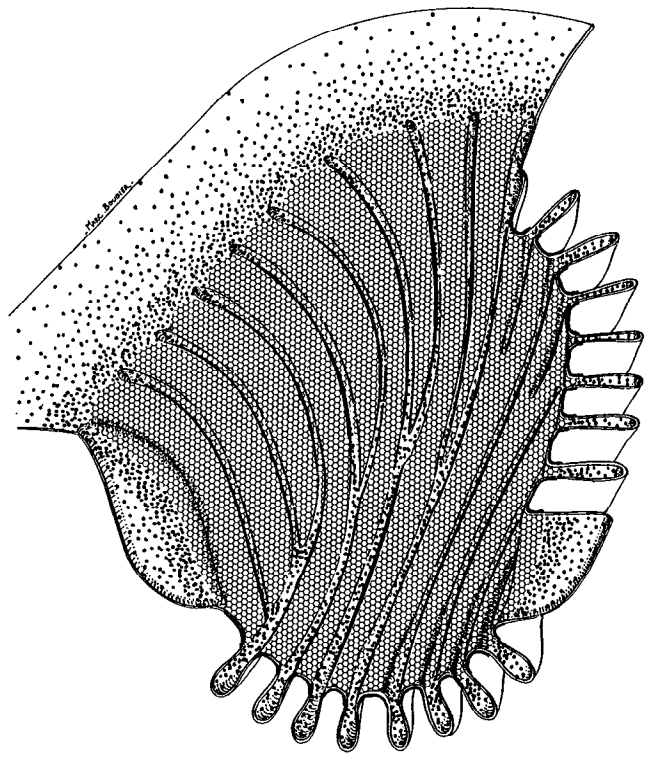

Figure 7. Schematic 3D view of the NMJ postsynaptic membrane with the nerve ending pulled off, illustrating the proposed Na^+ channel distribution (adapted from Couteaux, 1972). The fold crests, which contain a very high density of AChRs, cover almost the whole surface of the gutter facing the presynaptic membrane (hexagonal array). The other membrane domain, rich in Na^+ channels (*black dots*), includes the fold bottom and the perisynaptic membrane. Na^+ channel density is highest along the border of the AChR domain and decreases moving away. This figure shows how the high perisynaptic Na^+ channel density is explained by the fold ends on the gutter edge.

more, Na^+ channel density may be higher in the upper part of the bottom zone near the border with the AChR domain.

Na^+ channel distribution on presynaptic structures

The considerable Na^+ channel density on glial membranes contrasts with the low density or absence of Na^+ channels on the axonal membrane. Similar presynaptic distributions were observed on preparations submitted to a continuous 30 min rinse after incubation, in which most of the label was localized on glial cells (Boudier et al., 1988). The only difference between the Na^+ channel distribution on presynaptic structures observed here and those observed after long rinses is that source density in the glial–axonal membrane zone (see Table 1) was almost threefold higher than in the glial membrane alone (Tables 3, 4). Among the possible explanations, the most likely is that brief rinses were too short to wash out unbound ^{125}I-αScTx molecules trapped in the narrow space between the two membranes. This explanation supports the simple idea that while distribution of Na^+ channels on glia and axon is uniform, density is high only on the glial membrane (Boudier et al., 1988). Presence of Na^+ channels on Schwann cells has already been shown both *in vitro* (Chiu et al., 1984; Shrager et al., 1985) and *in vivo* (Ritchie and Rang, 1983; Chiu, 1987). However, the density reported here is much greater than previously reported (Ritchie, 1987). The Na^+ channel density on perisynaptic glial cells could be estimated at $\approx 1000/\mu m^2$ (Table 4) under the assumption that αScTx affinity is identical for glial and muscle membranes. Even in case of a much higher affinity of αScTx for glia than muscle, Na^+ channel density on teloglial cells should support excitability. An increase in potassium concentration in the synaptic cleft is able to induce depolarization of the glial cell membrane (reviewed in Kuffler et al., 1984). It is thus highly probable that depolarization invades perisynaptic glial cells in response to repetitive action potentials in nerve endings. The functional consequences of this phenomenon may be important (Boudier et al., 1988).

Very low labeling of both Ranvier nodes and unmyelinated axons in the mouse sciatic nerve has been observed with αScTx used alone (Massacrier et al., 1990). Labeling was enhanced by incubation in the presence of batrachotoxin and TTX, allowing these authors to conclude that low labeling was due partially to nerve membrane depolarization. The absence of labeling of the nerve ending membrane agrees with this observation and could be attributed to the same cause. Conversely, β-scorpion toxin (βScTx) has been successfully used as a probe for neuronal Na^+ channels in the PNS (Massacrier et al., 1990). New experiments using ^{125}I-βScTx are being conducted

Table 5. Na^+ channel distribution on postsynaptic folds

Hypothetical Na^+ channel distribution			Model source (number and limits)	Test against observed grains	
				χ^2	p (df = 7)
Uniform density over folds			1. Band 0–6 HD	18.34	<0.025
Absence on fold crests	Uniform density on bottoms		2. Band 2–6 HD	3.61	>0.75
	Nonuniform density on bottoms	Density higher in the end	3. Two bands: 2–6 HD, 4–6 HD	19.40	<0.01
		Density higher near crests	4. Two bands: 2–4 HD, 2–6 HD	1.77	>0.95
		Idem. steeper gradient	5. Four bands: 2–3 to 2–6 HD	2.50	>0.75

to study Na^+ channel distribution on presynaptic structures and may provide new insight into Na^+ channels on nerve ending membrane and perisynaptic glial cells.

Na^+ channel distribution on postsynaptic membranes

A preliminary question is whether the αScTx-binding sites visualized here are representative of the population of muscle Na^+ channels. Since TTX-resistant channels are undetectable in innervated adult muscle (Caldwell and Milton, 1988), they can be ruled out. Other muscle Na^+ channel subtypes (Haimovich et al., 1984, 1987) have been observed, and the possibility that one or several of these subtypes is not bound by αScTx cannot be excluded. However, no subtype difference between the synaptic–perisynaptic zone and the rest of the surface has been reported. It should also be noted that the distribution described here is roughly in accord with previous immunocytochemical localizations (Haimovich et al., 1987; Flucher and Daniels, 1989), the distribution of βScTx-binding sites at light microscopic level (Le Treut et al., 1990), and the perisynaptic Na^+ current high density (Beam et al., 1985; Caldwell et al., 1986; Caldwell and Milton, 1988). Thus, it appears reasonable to speculate that αScTx-binding site and Na^+ channel distributions are equivalent in muscle post- and perisynaptic membranes.

The perisynaptic membrane exhibited the highest Na^+ channel density, $\approx 5000/\mu m^2$. It was about twofold the density estimated on Ranvier nodes from electrophysiological measurements (Hille, 1984) and up to half the AChR density on fold crests. However, this density is in good agreement with the Na^+ current density recorded in the end-plate region, which greatly exceeded 100 mA/cm^2, reaching in some places 400 mA/cm^2 (Caldwell et al., 1986). On the simple assumption that current density scales with channel density, Caldwell et al. (1986) estimated the Na^+ channel density on the NMJs to be up to $\approx 8000/\mu m^2$. Nevertheless, Na^+ current measurements on the end-plate are in agreement with an Na^+ channel density higher than $2000/\mu m^2$ (Caldwell et al., 1986; Caldwell and Milton, 1988). If the ratio of Na^+ channel density on extrasynaptic muscle surface to that in areas close to the NMJ is considered to be between 1:7 (Le Treut et al., 1990) and 1:20 (Caldwell et al., 1986; Caldwell and Milton, 1988), our estimation of density would be in good agreement with the Na^+ channel density on the extrasynaptic muscle membrane, which was $175/\mu m^2$ with TTX binding (Jaimovich et al., 1976) and $200–500/\mu m^2$ with saxitoxin binding (Ritchie and Rogart, 1977; Hansen Bay and Strichartz, 1980). Such high Na^+ channel densities disagree with previous estimations based on ARG of ScTx-binding sites, that is from 5–10 sites/μm^2 on extrajunctional muscle surface to 40–80 sites/μm^2 in a 5-μm-wide perisynaptic area (Le Treut et al., 1990). These low values were calculated using previously published efficiency factors, which were probably not suited to our experimental conditions. Using the density reported here, that is, ≈ 5000 Na^+ channels/μm^2 close to the synaptic gutter, Na^+ channel density on extrajunctional muscle membrane area would be 400–700 Na^+ channels/μm^2.

With regard to Na^+ channel distribution, postsynaptic folds can be divided into two clearly distinguishable domains: fold crests and fold bottoms. Fold crests exhibit few or no Na^+ channels while fold bottoms exhibit a high density. Localization of Na^+ channels exclusively in the fold bottom has already been observed by immunocytochemistry (Flucher and Daniels, 1989). Our data showed that two distributions were possible for Na^+ channels in the fold bottom. The first is a uniform distribution in which mean density is lower than in perisynaptic areas bordering the gutters. However, the best-fit model is one in which density is twofold greater in the upper half than the lower half of the fold bottom (Table 5). In this case the density bordering the crest domain in folds would be identical to the density found on the perisynaptic edge. Thus, the membrane of the fold bottom and the perisynaptic membrane should be considered as the same membrane domain, with a decrease of Na^+ channel density moving either down into the fold or away from the gutter edge. The ends of the fold crests on the edge of the synaptic gutter could account for the high-density perisynaptic zone (Fig. 7).

In the muscle membrane, AChRs are tightly clustered on the crests of the synaptic folds, reaching a density as high as $10,000/\mu m^2$ (Heuser and Salpeter, 1979; Hirokawa and Heuser, 1982). Overall AChR density on the other muscle membrane domains is at least 500-fold lower. However, AChRs are not evenly distributed in these low-density domains. Moving down the fold bottom, AChR density varies from 9% to 3% of that in the crests (Fertuck and Salpeter, 1976). There is also a perisynaptic zone 25–50 μm wide, in which AChR density decreases regularly with distance from the edge of the synaptic cleft (Salpeter et al., 1988).

Thus, two distinct domains can be distinguished on the muscle membrane. The first is the fold crests, where the cytoplasmic side of the membrane is surrounded by a line of electron-dense material. This domain, which extends ≈ 0.2 μm down the fold (Fertuck and Salpeter, 1976; present results), contains AChRs at very high density (reviewed in Salpeter, 1987) and virtually no Na^+ channels (Flucher and Daniels, 1989; present results).

The second domain comprises the fold bottom and the perisynaptic membrane, beginning at the border of the thickened membrane. This domain contains numerous Na^+ channels, either uniformly distributed in folds with the highest density on the gutter edge, or more likely with a density twofold higher in a strip about 2 μm wide along the border of the AChR domain than in the adjacent 2 μm strip. On the perisynaptic surface, this domain extends 25–50 μm from the synaptic cleft (Salpeter et al., 1988; Le Treut et al., 1990) with decreasing Na^+ channel density (Fig. 7). AChRs are present at a much lower density, but their distribution is similar to those of Na^+ channels in the best-fit model (Salpeter et al., 1988). Since there is not a clear-cut limit between the perisynaptic zone and the extrasynaptic muscle cell surface, these two zones can be considered as a single membrane domain even though they differ with regard to excitability and conduction characteristics.

Both AChRs and Na^+ channels are bound to proteins that link them to the underlying cytoskeleton. In the *Torpedo* electroplaque membrane, a 43 kDa protein is associated with AChRs (reviewed in Froehner, 1986). The same protein is also colocalized with AChRs on the fold crests (Flucher and Daniels, 1989). Brain Na^+ channels are bound by ankyrin (Davis and Bennett, 1984; Srinivasan et al., 1988; reviewed in Morrow, 1989), which was localized exclusively in the fold bottom and in the perisynaptic membrane (Flucher and Daniels, 1989). These findings are in agreement with the hypothesis that the distribution of the AChRs and Na^+ channels within the end-plate results from immobilization in the membrane by anchor proteins. Anchoring of Na^+ channels by ankyrin could explain the high perisynaptic density. It could also account for the contrast between the low mobility of synaptic Na^+ channels and the relative mobility of the extrajunctional Na^+ channels (Angelides, 1986; Angelides et al., 1988; Milton and Caldwell, 1990). The coexistence of the density gradient with a proportion of mobile Na^+ channels in the perisynaptic membrane could be explained by the "binding site model" hypothesis recently proposed by Milton and Caldwell (1990).

The clear-cut division of the postsynaptic membrane into two distinct domains, one with AChRs and the other with Na^+ channels, has great implication for NMJ function. At the end-plate, ACh binding opens the AChR-associated channels and gives rise to the synaptic potential. ACh is released by quanta (Del Castillo and Katz, 1954). The release of a single quantum activates a very small area with a radius of $\approx$0.3 μm (Land et al., 1981), and the quantal current spreads over no more than $\approx$1 μm (Hartzell et al., 1975). A normal end-plate potential requires no more than 300 quanta randomly distributed on the receptive surface (Katz and Miledi, 1979). The muscle action potential supported by voltage-gated channels is triggered by the current spread from activated synaptic areas. Since it is devoid of Na^+ channels, the high-density AChR membrane cannot actively propagate depolarizations. Fold bottoms with high Na^+ channel density separate AChR-rich fold crests whose surface is $\approx$0.5 μm wide. This arrangement enables both maximal AChR density in the receptive area and close proximity between activated areas and Na^+ channel–rich membrane. The high Na^+ channel density in perisynaptic areas allows generation of the action potential by amplifying the initial depolarization triggered by synaptic currents. High Na^+ channel density has also been observed at the axon hillock, which is responsible for generating the action potential in central neurons of vertebrates (Wollner and Catterall, 1986). As already pointed out (Beam et al., 1985; Caldwell et al., 1986), the high density of Na^+ channels enhances the safety factor for impulse propagation.

Conclusion

Distribution analysis of ^{125}I-αScTx–labeled Na^+ channels under conditions allowing labeling of both pre- and postsynaptic channels showed that the postsynaptic membrane can be divided into two clear-cut membrane domains, as previously suggested on the basis of immunocytochemistry (Flucher and Daniels, 1989). The first domain is the thickened membrane of fold crests, which contains AChRs at very high density and few or no Na^+ channels. In the second domain, which extends from the border of fold crests to the end of the perisynaptic zone including the fold bottom, AChR density is very low and Na^+ channel density is high. Correlation of observed data with Na^+ channel distribution simulations suggested that Na^+ channel density may be maximal along the edge of the border between these two domains. Moving away from this border, Na^+ channel density decreases to the level of the extrasynaptic surface. These two postsynaptic membrane domains differ with regard to components and function. One supports reception and transduction of the chemical signal. The other allows generation of the action potential and initiation of its conduction.

References

Almers W, Stanfield PR, Stuhmer W (1983) Lateral distribution of sodium and potassium channels in frog skeletal muscle: measurements with a patch-clamp technique. J Physiol (Lond) 336:261–284.

Angelides KJ (1986) Fluorescently labelled Na^+ channels are localized and immobilized to synapses of innervated muscle fibres. Nature 321: 63–66.

Angelides KJ, Elmer LW, Elson E (1988) Distribution and lateral mobility of voltage-dependent sodium channels in neurons. J Cell Biol 106:1911–1925.

Ariyasu RG, Deerinck TJ, Levinson SR, Ellisman MH (1987) Distribution of $(Na^+ + K^+)$ATPase and sodium channels in skeletal muscle and electroplax. J Neurocytol 16:511–522.

Beam KG, Caldwell JH, Campbell DT (1985) Na channels in skeletal muscle concentrated near the neuromuscular junction. Nature 313: 588–590.

Betz WJ, Caldwell JH, Kinnamon SC (1984) Increased sodium conductance in the synaptic region of rat skeletal muscle fibres. J Physiol (Lond) 352:189–202.

Birks RI, Huxley HE, Katz B (1960) The fine structure of the neuromuscular junction of the frog. J Physiol (Lond) 150:134–144.

Blackett NM, Parry DM (1973) A new method for analyzing electron microscope autoradiographs using hypothetical grain distributions. J Cell Biol 57:9–15.

Blackett NM, Parry DM (1977) A simplified method of "hypothetical grain" analysis of electron microscope autoradiographs. J Histochem Cytochem 25:206–214.

Boudier JA, Berwald-Netter Y, Dellmann HD, Boudier JL, Couraud F, Koulakoff A, Cau P (1985) Ultrastructural visualization of Na^+-channel associated (^{125}I) alpha-Scorpion toxin binding sites on fetal mouse nerve cells in culture. Dev Brain Res 20:137–142.

Boudier JL, Jover E, Cau P (1988) Autoradiographic localization of voltage-dependent sodium channels on the mouse neuromuscular junction using ^{125}I-alpha scorpion toxin. I. Preferential labeling of glial cells on the presynaptic side. J Neurosci 8:1469–1478.

Caldwell JH, Milton RL (1988) Sodium channel distribution in normal and denervated rodent and snake skeletal muscle. J Physiol (Lond) 401:145–161.

Caldwell JH, Campbell DT, Beam KG (1986) Na channel distribution in vertebrate skeletal muscle. J Gen Physiol 87:907–932.

Cartaud J, Sobel A, Rousselet A, Devaux PF, Changeux J-P (1981) Consequences of alkaline treatment for the ultrastructure of the acetylcholine-receptor-rich membranes from *Torpedo marmorata* electric organ. J Cell Biol 90:418–426.

Catterall WA (1980) Neurotoxins that act on voltage-sensitive sodium channels in excitable membranes. Annu Rev Pharmacol Toxicol 20: 15–43.

Cau P (1988) BASIC programs to compute source densities from autoradiographic cross-fire matrices. J Microsc (Oxf) 150:199–209.

Cau P, Massacrier A, Boudier JL, Couraud F (1985) Ultrastructural localization of voltage-sensitive sodium channels using [^{125}I]alpha scorpion toxin. Brain Res 334:9–17.

Chiu SY (1987) Sodium currents in axon-associated Schwann cells from adult rabbits. J Physiol (Lond) 386:181–203.

Chiu SY, Shrager P, Ritchie JM (1984) Neuronal-type Na^+ and K^+ channels in rabbit cultured Schwann cells. Nature 311:156–157.

Couraud F, Rochat H, Lissitzky S (1978) Binding of scorpion and sea anemone neurotoxins to a common site related to the action potential Na^+ ionophore in neuroblastoma cells. Biochem Biophys Res Commun 83:1525–1530.

Couraud F, Jover E, Dubois JM, Rochat H (1982) Two types of scorpion toxin receptor sites, one related to the activation, the other to the inactivation of the action potential channel. Toxicon 20:9–16.

Couteaux R (1972) Motor end plate structure. In: Structure function of the muscle, Vol 1, part 1 (Bourne GH, ed), pp 483–530. New York: Academic Press.

Davis JQ, Bennett V (1984) Brain ankyrin. J Biol Chem 259:13550–13559.

Del Castillo J, Katz B (1954) Quantal components of the endplate potential. J Physiol (Lond) 124:560–573.

Downs A, Williams MA (1978) An iterative approach to the analysis of EM autoradiographs. I. The method. J Microsc (Oxf) 114:143–156.

Dreyfus P, Rieger F, Muravsky M, Garcia L, Lombet A, Fosset M, Pauron D, Barhanin J, Lazdunski M (1986) The voltage-dependent sodium channel is co-localized with the acetylcholine receptor at the vertebrate neuromuscular junction. Biochem Biophys Res Commun 139:196–201.

Duval A, Malecot CO, Pelhate M, Rochat H (1989) Changes in Na channel properties of frog and rat skeletal muscles induced by the AaH II toxin from the scorpion *Androctonus australis*. Pfluegers Arch Eur J Physiol 415:361–371.

Fertuck HC, Salpeter MM (1974) Sensitivity in electron microscope autoradiography for ^{125}I. J Histochem Cytochem 22:80–87.

Fertuck HC, Salpeter MM (1976) Quantitation of juctional and extrajunctional acetylcholine receptors by electron microscope autoradiography after ^{125}I-alpha bungarotoxin binding at mouse neuromuscular junction. J Cell Biol 69:144–158.

Flucher BE, Daniels MP (1989) Distribution of Na^+ channels and ankyrin in neuromuscular junctions is complementary to that of acetylcholine receptors and the 43 Kd protein. Neuron 3:163–175.

Froehner SC (1986) The role of the postsynaptic cytoskeleton in AChR organization. Trends Neurosci 9:37–40.

Haimovich B, Bonilla E, Casadei J, Barchi R (1984) Immunocytochemical localization of the mammalian voltage-dependent sodium channel using polyclonal antibodies against the purified protein. J Neurosci 4:2259–2268.

Haimovich B, Scotland DL, Fieles WE, Barchi RL (1987) Localization of sodium channel subtypes in adult rat skeletal muscle using channel-specific monoclonal antibodies. J Neurosci 7:2957–2966.

Hansen Bay CM, Strichartz GR (1980) Saxitoxin binding to sodium channels of rat skeletal muscles. J Physiol (Lond) 300:89–103.

Hartzell HC, Kuffler SW, Yoshikami D (1975) Post-synaptic potentiation: interaction between quanta of acetylcholine at the skeletal neuromuscular synapse. J Physiol (Lond) 251:427–463.

Heuser JE, Salpeter SR (1979) Organization of acetylcholine receptors in quick-frozen, deep-etched, and rotary replicated *Torpedo* postsynaptic membrane. J Cell Biol 82:150–173.

Hille B (1984) Ionic channels of excitable membranes. Sunderland, MA: Sinauer.

Hirokawa N, Heuser JE (1982) Internal and external differentiations of the postsynaptic membrane at the neuromuscular junction. J Neurocytol 11:487–510.

Jaimovich E, Venosa RA, Shrager P, Horowicz P (1976) Density and distribution of tetrodoxin receptors in normal and detubulated frog sartorius muscle. J Gen Physiol 67:399–416.

Jover E, Martin-Moutot N, Couraud F, Rochat H (1978) Scorpion toxin: specific binding to rat synaptosomes. Biochem Biophys Res Commun 85:377–382.

Katz B, Miledi R (1979) Estimates of quantal content during chemical potentiation of transmitter release. Proc R Soc Lond [Biol] 205:369–378.

Kuffler SW, Nicholls JG, Martin AR (1984) From neuron to brain. Sunderland, MA: Sinauer.

Land BR, Podleski TR, Salpeter EE, Salpeter MM (1977) Acetylcholine receptor distribution on myotubes in culture correlated to acetylcholine sensitivity. J Physiol (Lond) 269:155–176.

Land BR, Salpeter EE, Salpeter MM (1981) Kinetics parameters for acetylcholine interaction in intact neuromuscular junction. Proc Natl Acad Sci USA 78:7200–7204.

Larra F, Droz B (1970) Techniques radioautographiques et leur application à l'étude du renouvellement des constituants cellulairs. J Microsc (Paris) 9:845–880.

Le Treut T, Boudier JL, Jover E, Cau P (1990) Localization of voltage-sensitive sodium channels on the extrasynaptic membrane surface of the mouse skeletal muscle by autoradiography of scorpion toxin binding sites. J Neurocytol 19:408–420.

Marchot P, Frachon P, Bougis PE (1988) Selective distinction at equilibrium between the two alpha-neurotoxin binding sites of *Torpedo* acetylcholine receptor by microtitration. Eur J Biochem 174:537–542.

Martin MF, Perez LGG, El Ayeb M, Kopeyan C, Bechis G, Jover E, Rochat H (1987) Purification and chemical and biological characterizations of seven toxins from the Mexican scorpion, *Centruroides suffusus suffusus*. J Biol Chem 262:4452–4459.

Massacrier A, Couraud F, Cau P (1990) Voltage-sensitive Na^+ channels in mammalian peripheral nerves detected using scorpion toxins. J Neurocytol 19:850–872.

McArdle JJ (1984) Overview of the physiology of the neuromuscular junction. In: The neuromuscular junction (Brumback RA, Gerst JW, eds), pp 65–119. New York: Futura.

McArdle JJ, Angaut-Petit D, Mallart A, Bournaud R, Faille L, Brigant JL (1981) Advantages of the triangularis sterni muscle of the mouse for investigations of synaptic phenomena. J Neurosci Methods 4:109–115.

Milton RL, Caldwell JH (1990) Na current in membrane blebs: implications for channel mobility and patch-clamp recording. J Neurosci 10:885–893.

Morrow JS (1989) The spectrin membrane skeleton: emerging concepts. Curr Op Cell Biol 1:23–29.

Poli MA, Mende TJ, Baden DG (1986) Brevetoxins, unique activators of voltage-sensitive sodium channels, bind to specific sites in rat brain synaptosomes. Mol Pharmacol 30:129–135.

Ritchie JM (1987) Voltage-gated cation and anion channels in mammalian Schwann cells and astrocytes. J Physiol (Paris) 82:248–257.

Ritchie JM, Rang HP (1983) Extraneuronal saxitoxin binding sites in rabbit myelinated nerve. Proc Natl Acad Sci USA 80:2803–2807.

Ritchie JM, Rogart RB (1977) The binding of a labelled saxitoxin to the sodium channels in normal and denervated mammalian muscle and in amphibian muscle. J Physiol (Lond) 269:341–354.

Rochat H, Gregoire J, Martin-Moutot N, Menashe M, Kopeyan C, Miranda F (1974) Purification of animal neurotoxins: isolation and characterization of three neurotoxins from the venom of *Naja nigricollis mossambica* Peters. FEBS Lett 42:335–339.

Salpeter MM (1987) Vertebrate neuromuscular junctions: general morphology, molecular organization and functional consequences. In: The vertebrate neuromuscular junction (Salpeter MM, ed), pp 1–54. New York: Liss.

Salpeter MM, Bachmann L, Salpeter EE (1969) Resolution in electron microscope radioautography. J Cell Biol 41:1–20.

Salpeter MM, Fertuck HC, Salpeter EE (1977) Resolution in electron microscope autoradiography. III. Iodine-125, the effect of heavy metal staining, and a reassessment of critical parameters. J Cell Biol 72: 161–173.

Salpeter MM, McHenry FA, Salpeter EE (1978) Resolution in electron microscope autoradiography. IV. Application to analysis of autoradiographs. J Cell Biol 76:127–145.

Salpeter MM, Smith CD, Matthews-Bellinger JA (1984) Acetylcholine receptor at neuromuscular junctions by EM autoradiography using mask analysis and linear sources. J Elec Microsc Tech 1:63–81.

Salpeter MM, Marchaterre M, Harris R (1988) Distribution of extrajunctional acetylcholine receptors on a vertebrate muscle: evaluated by using a scanning electron microscope autoradiographic procedure. J Cell Biol 106:2087–2093.

Sealock R (1982) Cytoplasmic surface structure in postsynaptic membranes from electric tissue visualized by tannic acid–mediated negative contrasting. J Cell Biol 92:514–522.

Sherman SJ, Lawrence JC, Messner DJ, Jacoby K, Catterall WA (1983) Tetrodotoxin-sensitive sodium channels in rat muscle cells developing *in vitro*. J Biol Chem 258:2488–2495.

Shrager P, Chiu SY, Ritchie JM (1985) Voltage dependent sodium and potassium channels in mammalian cultured Schwann cells. Proc Natl Acad Sci USA 82:948–952.

Small JV (1968) Measurements of section thickness. In: Proceedings of the fourth European Congress on Electron Microscopy, Vol 1 (Bocciarelli DS, ed), p 609. Rome: Poliglotta Vaticana.

Srinivasan Y, Elmer L, Davis J, Bennett V, Angelides K (1988) Ankyrin and spectrin associate with voltage-dependent sodium channels in brain. Nature 333:177–180.

Thomsen WJ, Catterall WA (1989) Localization of the receptor site for alpha-scorpion toxins by antibody mapping—implications for sodium channel topology. Proc Natl Acad Sci USA 86:10161–10165.

Weibel ER (1979) Stereological methods, Vol 1, Practical methods for biological morphometry. London: Academic.

Williams MA (1977) The analysis of electron microscope autoradiographs. In: Quantitative methods in biology: practical methods in electron microscopy, Vol 6 (Glauert AM, ed), pp 85–169. Amsterdam: North-Holland.

Williams MA, Downs A (1978) An iterative approach to the analysis of EM autoradiographs. II. Estimates of sample sizes confidence limits. J Microsc (Oxf) 114:157–178.

Wollner DA, Catterall WA (1986) Localization of sodium channels in axon hillocks and initial segments of retinal ganglion cells. Proc Natl Acad Sci USA 83:8424–8428.